

## Sensors

## Spatiotemporal Measurement of Osmotic Pressures by FRET Imaging

Wenbo Zhang, Luca Bertinetti, Kerstin G. Blank, Rumiana Dimova, Changyou Gao, Emanuel Schneck,\* and Peter Fratzl\*

**Abstract:** Osmotic pressures (OPs) play essential roles in biological processes and numerous technological applications. However, the measurement of OP *in situ* with spatiotemporal resolution has not been achieved so far. Herein, we introduce a novel kind of OP sensor based on liposomes loaded with water-soluble fluorescent dyes exhibiting resonance energy transfer (FRET). The liposomes experience volume changes in response to OP due to water outflux. The FRET efficiency depends on the average distance between the entrapped dyes and thus provides a direct measure of the OP surrounding each liposome. The sensors exhibit high sensitivity to OP in the biologically relevant range of 0–0.3 MPa in aqueous solutions of salt, small organic molecules, and macromolecules. With the help of FRET microscopy, we demonstrate the feasibility of spatiotemporal OP imaging, which can be a promising new tool to investigate phenomena involving OPs and their dynamics in biology and technology.

## Introduction

The conversion of chemical into mechanical energy is an essential function in all living systems as well as in many technical processes. Molecular motors are essential components of cells that generate force by burning ATP, the cell-internal fuel. Within our muscles, molecular motors are responsible for animal locomotion, but they also mediate cell motility and adhesion and many other cellular processes. In plants, force generation and organ movement is often linked to turgor pressure, which is generated by another type of chemo-mechanical conversion based on osmotic gradients. These are known for more than hundred years<sup>[1]</sup> to be critical for a variety of cell functions,<sup>[2]</sup> living tissue organizations<sup>[3]</sup> and vital activities.<sup>[4]</sup> Osmotic pressure is recognized as an

How to cite: *Angew. Chem. Int. Ed.* **2021**, *60*, 6488–6495  
International Edition: doi.org/10.1002/anie.202011983  
German Edition: doi.org/10.1002/ange.202011983

important biophysical cue as it can induce cell volume changes, which in turn activate osmoregulatory responses<sup>[4]</sup> and can determine, for example, stem cell fate.<sup>[5]</sup> Moreover, osmotic gradients are exploited by bacteria to promote spreading of colonies and to outcompete the growth of other cells.<sup>[6]</sup> In many cases, osmotic pressure is regulated for mechanical purposes: plants are well known to use osmotic pressure to create turgor for cell expansion and organ movements, such as the opening of a flower.<sup>[7]</sup> Another example is cartilage, which is stabilized by the swelling pressure of proteoglycans counter-balanced by the tension of (type II) collagen.<sup>[3,8]</sup> For example, in intact joints, there is a gentle grading of fixed charge density of cartilage and hence of osmotic pressure from the articular surface to the deep zone.<sup>[3,9]</sup> In addition, static and dynamic osmotic pressure gradients also occur in many other contexts from soil sciences,<sup>[10]</sup> to colloidal sciences,<sup>[11]</sup> water treatment,<sup>[12]</sup> energy generation,<sup>[13]</sup> material engineering,<sup>[14]</sup> and membrane filtration.<sup>[15]</sup>

In contrast to molecular motors, the functions of which have been studied in great detail,<sup>[16]</sup> much less is known about the potential roles of osmotic pressures, especially in animal tissues. One of the reasons is the lack of *in situ* probes for osmotic strength sensing. Such sensors would not only be important in biological contexts but also in all situations where osmotic processes need to be monitored *in-operando* from biology to physical chemistry and to engineering. The goal of the present work is to develop a local probe for spatiotemporal monitoring of osmotic stresses through light microscopy.

At present, the osmotic strength of homogeneous solutions is usually determined by measuring and analyzing colligative properties of the solutions, such as freezing-

[\*] Dr. W. Zhang, Dr. L. Bertinetti, Prof. P. Fratzl  
Department of Biomaterials,  
Max Planck Institute of Colloids and Interfaces  
14476 Potsdam (Germany)  
E-mail: Peter.Fratzl@mpikg.mpg.de

Dr. K. G. Blank  
Mechano(bio)chemistry,  
Max Planck Institute of Colloids and Interfaces  
14476 Potsdam (Germany)

Dr. R. Dimova  
Department of Theory & Bio-Systems,  
Max Planck Institute of Colloids and Interfaces,  
14476 Potsdam (Germany)

Prof. C. Gao  
MOE Key Laboratory of Macromolecular Synthesis and  
Functionalization, Department of Polymer Science and Engineering,  
Zhejiang University, Hangzhou 310027 (China)

Prof. E. Schneck  
Department of Biomaterials,  
Max Planck Institute of Colloids and Interfaces  
14476 Potsdam (Germany)  
and  
Department of Physics, Technische Universität Darmstadt  
64289 Darmstadt (Germany)  
E-mail: schneck@fkp.tu-darmstadt.de

Supporting information and the ORCID identification number(s) of the author(s) of this article can be found under:  
<https://doi.org/10.1002/anie.202011983>.

© 2020 The Authors. *Angewandte Chemie International Edition* published by Wiley-VCH GmbH. This is an open access article under the terms of the Creative Commons Attribution Non-Commercial License, which permits use, distribution and reproduction in any medium, provided the original work is properly cited and is not used for commercial purposes.

point<sup>[17]</sup> and vapor-pressure depression.<sup>[18]</sup> Alternatively, the osmotic pressure can be measured by a setup composed of manometers and semipermeable membranes.<sup>[19]</sup> However, these conventional methods have no spatial resolution and are therefore inapplicable to measurements of osmotic pressures in situ or in vivo. Therefore, a method for the spatiotemporal measurement of the osmotic pressure remains highly desirable.

Phospholipid liposomes exhibit permeability properties similar to those of biological membranes,<sup>[20]</sup> which constitute semi-permeable barriers capable of creating and maintaining defined osmotic pressures required for cellular activities.<sup>[21]</sup> On timescales of seconds to hours, liposomes are water-permeable but vastly impermeable to ions, macromolecules, and most water-soluble molecules. Compared with semi-permeable polymer microcapsules<sup>[22]</sup> and polymer membranes (polymerosomes),<sup>[23]</sup> liposomes are highly deformable due to the low bending rigidity of lipid bilayers,<sup>[24]</sup> especially when composed of lipids with un-saturated alkyl chains.<sup>[25]</sup> In fact, various studies have demonstrated the response of liposomes to external osmotic pressures in terms of volume and shape changes.<sup>[17,25,26]</sup> With that, liposomes lend themselves towards their application as sensitive osmotic pressure sensors.

FRET (Förster resonance energy transfer), the nonradiative transfer of excitation energy from an excited donor dye to a proximal ground-state acceptor dye,<sup>[27]</sup> has been employed

to design various fluorescence-based sensors.<sup>[28]</sup> FRET occurs when donor and acceptor dyes are in nanometric proximity, in which case the donor fluorescence emission is decreased, and the acceptor emission is increased (sensitized emission). The method is ratiometric and thus eliminates ambiguities due to the measurement geometry, the probe concentration, etc., by self-calibration of two emission bands.<sup>[28a,29]</sup> Donors and acceptors that are covalently linked, free in solution, or contained in restricted geometries, have been used to study macromolecule structures, interactions, and crowding, and to detect analytes or hydrogel deformation, etc.<sup>[30]</sup> For free dyes in solution, diffusion significantly enhances the energy transfer efficiency, such that considerable FRET is observed even for comparatively low dye concentrations.<sup>[31]</sup> By combining FRET with optical microscopy it is possible to obtain quantitative spatiotemporal information on intra- and inter-molecular distances.<sup>[29c,32]</sup> In fact, ratiometric FRET sensors have previously been used to quantify macromolecular crowding in living cells,<sup>[33]</sup> an aspect that is related to osmotic pressure effects.

Here, we introduce FRET-based sensors for the direct quantification of osmotic pressures (Figure 1a). They are based on liposomes loaded with two highly water-soluble FRET dyes, ATTO 488 and ATTO 542. POPC (1-palmitoyl-2-oleoyl-glycero-3-phosphocholine), a typical naturally-occurring monounsaturated phospholipid forming liquid-crystalline bilayers at all relevant temperatures,<sup>[34]</sup> was chosen as

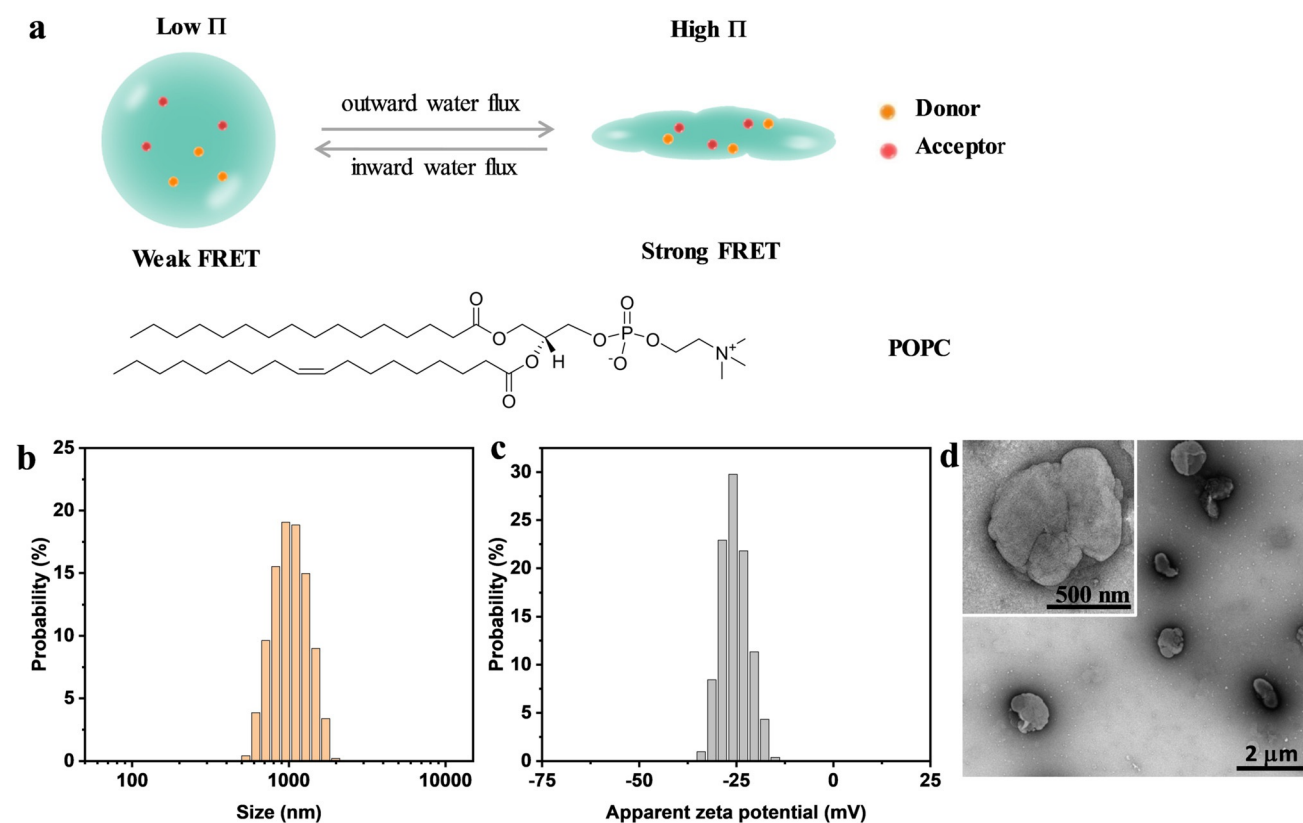


**Figure 1.** Osmotic pressure sensors based on dye-loaded liposomes (POPC-D-A). a) Schematic illustration of the working principle: The osmotic pressure  $\Pi$  leads to liposome shrinkage and thus to closer donor–acceptor proximity, enhancing FRET. b,c) Distributions of size (b) and zeta potential (c) of POPC-D-A liposomes in water as obtained by dynamic light scattering (DLS) and phase analysis light scattering (PALS), respectively. d) TEM images of POPC-D-A liposomes in dry state (inset, higher magnification) stained with 1% uranyl acetate.

the constituent of the semipermeable liposome membrane. The intra-liposomal dye concentration was chosen to be  $50\ \mu\text{M}$ . The associated sensor-inherent osmotic pressure ( $\lesssim 1\ \text{kPa}$ ) is negligible compared to the external osmotic pressures investigated. The sensitivity and applicable pressure range of the sensors depend on two specific features. The first one is the liposomes' relative volume change upon exposure to osmotic pressure  $\Pi$ , determined by the liposome size as well as the bending and stretching elastic properties of the constituting lipid bilayers. The second one is the response of the FRET efficiency, measured in the form of the (sensitized acceptor emission)/(donor emission) ratio  $R$ , to the resulting intra-liposomal dye concentration changes. Both features taken together can be conveniently mapped onto a “ $R$  versus  $\Pi$ ”-calibration curve based on which the osmotic pressure at a sensor's position in an unknown environment is obtained from a simple measurement of the FRET efficiency. Combined with FRET microscopy, this procedure enables spatio-temporal osmotic pressure imaging.

## Results and Discussion

Dye-loaded liposomes were prepared by a simple extrusion method (Figure S1). Dry POPC thin films on the inner walls of a glass vial were first hydrated with a mixed aqueous solution of ATTO 488 (donor) and ATTO 542 (acceptor) dyes, resulting in multilamellar aggregates. Liposomes containing the donor (“D”) and acceptor (“A”) dyes, termed

“POPC-D-A” in the following, were then obtained by extrusion (see SI) and removal of extra-liposomal free dyes was achieved via rinsing and centrifugation. The average hydrodynamic diameter in water, as measured by dynamic light scattering (DLS) was  $\approx 1\ \mu\text{m}$  (Figure 1b). The zeta potential (Figure 1c) was found to be  $\approx -25\ \text{mV}$ , similar to that of POPC liposomes without dye loading (Figure S2) and consistent with earlier reports.<sup>[35]</sup> Transmission electron microscopy (TEM) images show that some POPC-D-A liposomes are multi-lamellar and multi-compartmented (Figure 1d); however the morphology may change upon drying.

ATTO 488 ( $\text{MW} = 804\ \text{g mol}^{-1}$ ) and ATTO 542 ( $\text{MW} = 1028\ \text{g mol}^{-1}$ ) were chosen as the donor and acceptor fluorophores, respectively, because of their excellent water solubility, high fluorescence quantum yield and high photostability,<sup>[36]</sup> as well as negligible interaction with zwitterionic lipid bilayers.<sup>[37]</sup> Moreover, the fluorescence spectrum of ATTO 488 and the absorption spectrum of ATTO 542 in water show considerable overlap (Figure 2a), which is a prerequisite for FRET.<sup>[38]</sup> The strong dependence of the FRET efficiency on the distance between donors and acceptors<sup>[38]</sup> (as the inverse sixth power of the distance) constitutes the basis for the utility of this phenomenon in sensing. In an aqueous solution of FRET pair dyes at a fixed stoichiometry, the donor-acceptor distances are relevant with the dye concentration. To study the sensitivity of the FRET efficiency between ATTO 488 and ATTO 542 to volume (i.e. distance) changes, the fluorescence spectra of aqueous ATTO 488, ATTO 542 and 1:1 mixed solutions were measured for a series

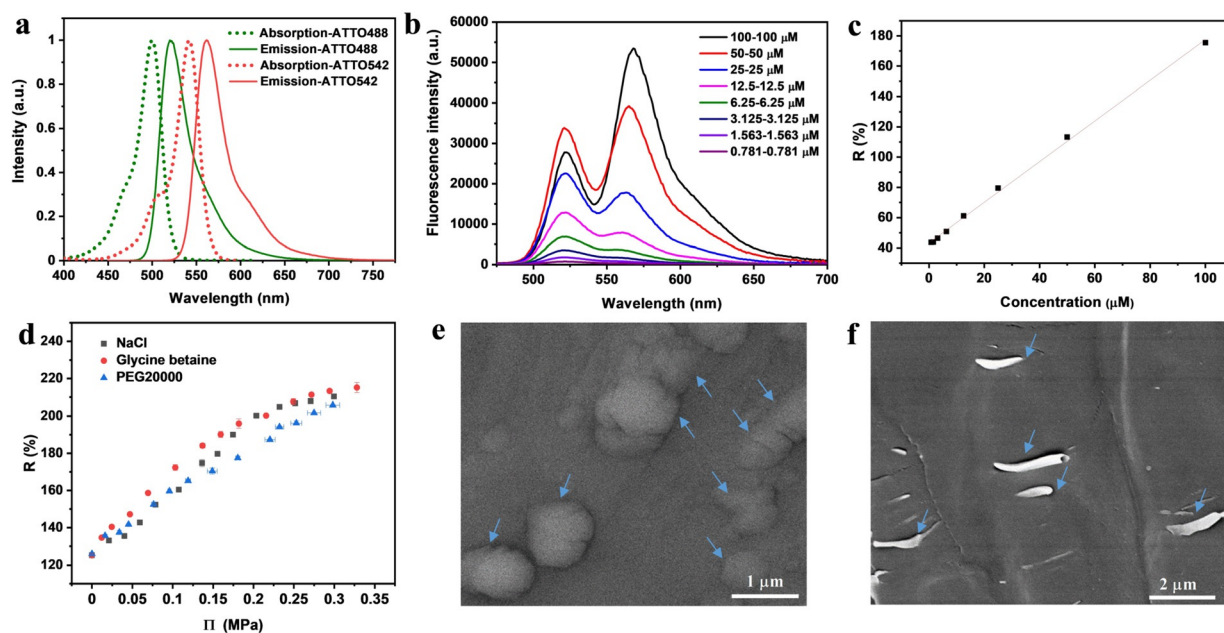


**Figure 2.** Sensing of osmotic pressures. a) Normalized UV/Vis absorption spectra and fluorescence emission spectra of ATTO 488 (donor) and ATTO 542 (acceptor) dyes in water. b) Fluorescence emission spectra of ATTO 488—ATTO 542 mixture (1:1 molar ratio) in water with different concentrations (0.781–100  $\mu\text{M}$ ) at a fixed excitation wavelength of 440 nm. c) Emission ratio  $R$  as a function of the dye concentration in a 1:1 molar ratio in bulk aqueous solution. The solid line is a linear fit to the data points (coefficient of determination = 0.998). d)  $R$  obtained with POPC-D-A liposomes loaded with a dye concentration of  $50\ \mu\text{M}$  (1:1 molar ratio) as a function of the external osmotic pressure generated by various concentrations of NaCl, GB, or PEG. The excitation wavelength was 440 nm. e,f) Cryo-SEM images of POPC-D-A liposomes in water (e) and NaCl solution (0.35%, 0.27 MPa) (f). Blue arrows indicate individual POPC-D-A liposomes.

of concentrations, using a fixed excitation wavelength of  $\lambda = 440$  nm (Figure S3, Figure 2b).

In the fluorescence spectra of the mixtures, the contribution of the acceptor emission systematically increases relative to the donor emission with increasing concentration (Figure 2b). This observation clearly confirms the sensitized emission of the acceptor (ATTO 542). In order to quantify the FRET efficiency, the (sensitized acceptor emission)/(donor emission) ratio was used, defined here as the ratio between the emission intensities at 562 nm and 520 nm. In the following, this ratio is referred to as the emission ratio  $R$ . Figure 2c shows  $R$  as a function of the dye concentration in a 1:1 molar ratio, which is seen to increase monotonically with the concentration. In fact, in the investigated concentration range the increase is surprisingly linear. The solid line in Figure 2c is a linear fit (coefficient of determination = 0.998) with  $R = 43.33 + 1.34c$ , where  $c$  is the dye (donor/acceptor) molarity in  $\mu\text{M}$ . Excitation at 458 nm (Figure S4) gave similar results to those obtained with 440 nm excitation. Rough estimates of the average next neighbor distance between two dye molecules (assumed to behave as ideal solutes) and of the probability distribution of next neighbor distances confirms that donors and acceptors have a considerable probability to be relatively close to each other ( $< 10$  nm), see Supporting Information. Moreover the fluorophore diffusion and the fluorophore size effect (the diameter of a typical dye chromophore is 10–15 Å) can be considered to further promote small donor-acceptor distances.<sup>[31]</sup> Possible interactions between the donor and the acceptor fluorophores, such as electrostatic attraction, can influence the donor-acceptor distance and thus the FRET efficiency.<sup>[31a]</sup> However, these effects are empirically captured by the calibration curves based on which the emission ratios are interpreted.

In the following studies, a fixed dye concentration of 50  $\mu\text{M}$  (1:1 molar ratio) was used to prepare the dye-loaded POPC-D-A liposomes. To determine the osmotic response, sodium chloride (NaCl), the most abundant solute in extracellular fluid; glycine betaine (GB), a typical intracellular organic osmolyte able to stabilize proteins;<sup>[39]</sup> and polyethylene glycol (PEG, average MW = 20000  $\text{g mol}^{-1}$ ), an inert macromolecule widely used in the control of osmotic pressures,<sup>[26a,40]</sup> were used. For each solute type, a series of solutions with independently measured osmotic pressures were prepared (Figure S5). The POPC-D-A liposomes were then exposed to the respective solutions and the FRET efficiency was determined from the recorded fluorescence spectra. Figure 2d shows  $R$  of the intra-liposomal dyes as a function of the osmotic pressure in the range of  $0 \leq \Pi \leq 0.3$  MPa for all three solute types. At  $\Pi = 0$ , the emission ratio ( $R \approx 125\%$ ) is similar to the one in a bulk solution of the same dyes at 50  $\mu\text{M}$  ( $R \approx 115\%$ , see Figure 2c). This consistency indicates that the dyes partition approximately evenly inside and outside the liposomes during the preparation process and is in line with the ratiometric character of the FRET mechanism, which eliminates the influence of the sample geometry and of the overall amount of dye in a sample. The same consistency is observed when comparing liposomes loaded with 25  $\mu\text{M}$  dyes ( $R \approx 85\%$ , see Figure S6) with a 25  $\mu\text{M}$  bulk solution ( $R \approx 80\%$ , see Figure 2c).

Molecular energy transfer in general can occur via radiative and non-radiative mechanisms.<sup>[41]</sup> In the present case the non-radiative mechanism FRET can be considered dominant based on the above results and similar reported cases.<sup>[31a,b,42]</sup>

Irrespective of the solute type, the emission ratio  $R$  increases monotonically with  $\Pi$ , first approximately linearly at low pressures ( $\Pi \lesssim 0.2$  MPa) and then turning to a weaker pressure dependence at higher pressures ( $\Pi > 0.2$  MPa). In view of the virtually linear concentration dependence of  $R$  in bulk (Figure 2c), this observation indicates that the volumetric response of the liposomes to the external osmotic pressure is non-linear. The liposomes are more easily deformed when in their initial spherical shape than when already partially deflated, a behavior that must be attributed to the bending rigidity of the lipid bilayer. The shape changes of the liposomes were observed with cryo scanning electron microscopy (cryo-SEM), which showed that the original liposomes are nearly spherical in pure water (Figure 2e, indicated with blue arrows) and flattened at high osmotic pressures (Figure 2f, indicated with blue arrows). The disk-like shapes observed here are qualitatively consistent with those experimentally observed and theoretically predicted earlier under the assumption of conserved bilayer surface area.<sup>[17,26b,43]</sup> Assuming that the fluorophores inside the liposomes behave as in a bulk dye solution, the relative volume change (i.e., water loss) can be estimated from the bulk dye concentration at which the same emission ratio is observed. For example, for POPC-D-A liposomes subject to  $\Pi = 0.1$  MPa, where the emission ratio is  $R \approx 160\%$  (see Figure 2d), the equivalent dye bulk concentration is  $c_{\text{equiv}} \approx 85 \mu\text{M}$  (see Figure 2c). The associated volume reduction is then  $1 - c_0/c_{\text{equiv}} \approx 41\%$ , where  $c_0 = 50 \mu\text{M}$  is the dye loading concentration. The average fluorophore distance can be roughly estimated within the Wigner-Seitz approximation. Further taking into account the effects of fluorophore diffusion, size and interactions, the FRET probabilities can be estimated, if desired, with the help of specific statistical methods such as Gösele's theory.<sup>[31c]</sup>

Importantly, the emission ratio at a given osmotic pressure is consistent among the three solute types (Figure 2c). Minor deviations between PEG on one side and the two other solute types on the other side must be attributed to systematic uncertainties in the determination of the osmotic pressure, which is measured in different ways for macromolecules and small solutes (see Supporting Information). This result demonstrates that the POPC-D-A liposomes are equally impermeable to all osmotic agents investigated and thus exhibit the same response to osmotic stress irrespective of its source. Repeated experiments with the same batch of liposomes demonstrated good reproducibility of the osmotic sensing under the same conditions (Figure S7). The reversibility of the osmotic response was confirmed in re-dilution experiments (see Figure S8).

Taken together, the results obtained are in line with the schematic illustration of the osmotic pressure sensing principle in Figure 1a: The liposomes shrink due to the osmotically driven outward flux of water through the lipid bilayer, such that the dye concentration in the liposome cavity increases, and in turn the FRET efficiency. In fact, adjusting the bilayer bending rigidity, the spectral overlap between the fluoro-

phores chosen, the initial intra-liposomal dye concentration and loaded osmotically active solutes on the inside should allow producing sensors optimized for a wide range of osmotic pressures. For example, the osmotic pressure range can readily be extended towards physiological salt concentrations and beyond by loading liposomes with osmotically active solutes on the inside, as exemplarily shown for 0.1% NaCl (Figure S9). The increase in the range of accessible osmotic pressures comes, however, as a trade-off with sensitivity, as evidenced by the reduced slope of emission ratio versus osmotic pressure (Figure S9), which emphasizes the opportunity and the need for optimizing the sensors to the required pressure range.

With the sensing principle established, the possibility of spatiotemporal imaging of osmotic pressures with POPC-D-A liposomes was investigated. Confocal laser scanning microscopy (CLSM) was chosen for sensitized emission FRET imaging at an excitation wavelength of  $\lambda = 458$  nm (see SI for the details). At high magnification (eyepiece 630 $\times$ ), well-dispersed individual liposomes can be observed exhibiting donor emission, sensitized acceptor emission, and direct acceptor emission signals (Figure 3a). In the next step, a drop of POPC-D-A liposome suspension placed on a glass slide was imaged at lower magnification by exciting the donor fluorophores and recording the emission from the donor (donor signal, Figure 3b upper left panel) and the acceptor fluorophores (sensitized acceptor emission signal, Figure 3b upper right panel) separately. The direct acceptor emission (Figure 3b lower left panel) was probed via selective acceptor excitation with a longer wavelength ( $\lambda = 561$  nm). According to established procedures,<sup>[29d,32a,44]</sup> the FRET efficiency is then again measured in the form of the ratio  $R$  between the

sensitized acceptor emission and the donor emission for each pixel (Figure 3b lower right panel). Figure 3c shows emission ratio images of POPC-D-A-loaded droplets of NaCl solutions with systematically increasing NaCl concentrations corresponding to osmotic pressures in the range between 0 and  $\approx 0.31$  MPa. The emission ratio, averaged in a region of interest indicated with a red rectangle, is seen to increase systematically with increasing osmotic pressure, from  $R \approx 53\%$  (at  $\Pi = 0$ ) to  $R \approx 87\%$  (at  $\Pi \approx 0.31$  MPa). Quantitative analysis yielded a calibration curve (Figure 3d), whose shape is consistent with the one obtained in the spectrofluorometer (Figure 2d). Note, however, that the  $R$ -values obtained from the fluorescence microscopy cannot be quantitatively compared with those obtained from the fluorescence spectroscopy due to different collection and calculation methods of the signal. The spatial resolution at which the osmotic pressure can be imaged is mainly related to the average distance between individual sensor-liposomes in the sample and can be improved by increasing the liposome concentration.

In order to illustrate the feasibility of in situ mapping of spatially distributed osmotic pressures, two droplets of aqueous POPC-D-A liposome suspensions, one containing pure water and one containing a NaCl solution of  $\Pi = 0.285$  MPa, were first brought to proximity (see Figure 4a for the emission ratio image) and then brought to coalescence (Figure 4b). The spatially dependent distribution of emission ratio ( $R$ ) values reveals the transient formation of an osmotic pressure gradient (indicated with the yellow arrow) across the contact zone. Moreover, regions of elevated osmotic pressures can be clearly identified along the edges of the solution (indicated with white arrows). They can be considered

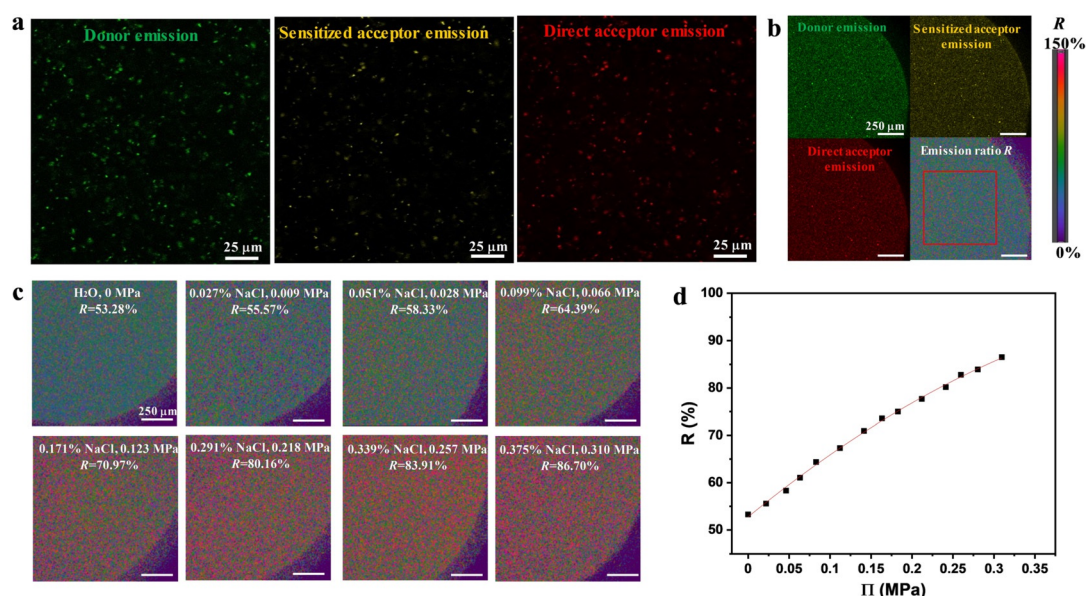


**Figure 3.** Application of POPC-D-A liposomes for osmotic pressure imaging. a) Confocal laser scanning microscopy (CLSM) images of individual POPC-D-A liposomes in water at high magnification, with the donor emission signal on the left (Ex 458 nm, Em 468–538 nm), the sensitized acceptor emission signal in the middle (Ex 458 nm, Em 571–700 nm), and the direct acceptor emission signal on the right (Ex 561 nm, Em 571–700 nm). b) CLSM images at lower magnification. The lower right image shows the emission ratio  $R$  in each pixel. c) Emission ratio ( $R$ ) images of POPC-D-A liposomes in NaCl solutions of various osmotic pressures. d) Calibration curve recorded at various osmotic pressures. The solid line is an empirical second-order polynomial fit to the data points (coefficient of determination = 0.998).

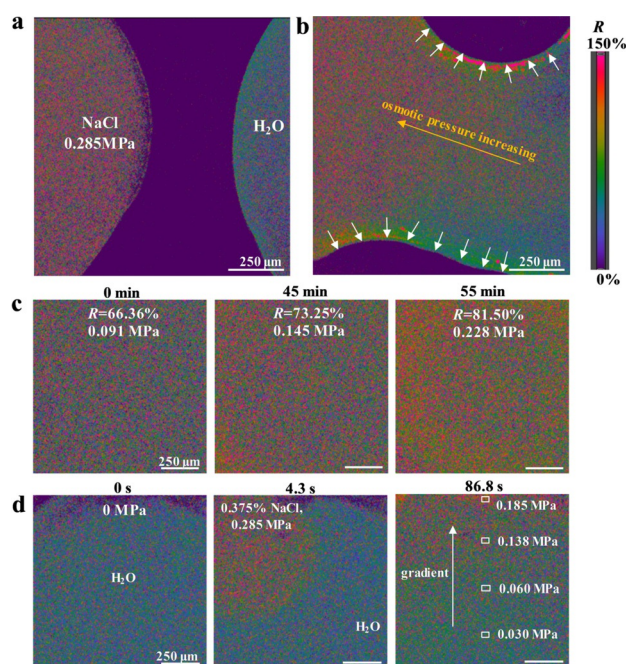


**Figure 4.** FRET imaging for the in situ spatiotemporal measurement of osmotic pressures. a) Emission ratio ( $R$ ) image of two droplets of aqueous POPC-D-A liposome suspensions with different osmotic pressures. They exhibit clearly different FRET efficiencies. b) Emission ratio ( $R$ ) image after droplet coalescence exhibiting distinct osmotic pressure gradients. c) Monitoring of osmotic pressure changes of a NaCl solution during evaporation process. d) Spatiotemporal imaging of an osmotic-pressure gradient generated through localized coalescence of a water drop and a drop of NaCl solution. The indicated osmotic pressures are calculated using the calibration curve (Figure 3 d).

manifestations of steep osmotic pressure gradients due to water evaporation under steady-state conditions.

In the next step, the in situ spatiotemporal measurement of osmotic pressures by time-lapse fluorescence imaging and subsequent quantitative analysis was further explored. To this end, the liposomes were used for real-time in situ monitoring of dynamically changing osmotic pressures during an evaporation process of NaCl solution. A drop of NaCl solution of moderate osmotic pressure ( $\Pi \approx 0.095$  MPa) containing POPC-D-A liposomes was placed on the glass bottom of a 20-mm dish with lid and let evaporate. Time-lapse fluorescence imaging shows that the emission ratio  $R$  increased gradually over time within 1 h (Figure 4c, Figure S10). With the calibration curve (Figure 3 d) at hand, the osmotic pressures were calculated and are indicated in Figure 4c. The solution concentrations (Table S1) were further calculated according to the osmotic pressure-mass fraction calibration curve (Figure S5d), where osmotic pressure and NaCl concentration were seen to increase monotonically with time. These results clearly demonstrate that the POPC-D-A liposome sensors can be used to measure dynamically changing osmotic pressures in situ. A possible disturbance of the liposome distribution in the droplets due to coffee-ring effect and Marangoni flow does not affect the measurement of osmotic pressures as a result of the ratio-metric character of FRET microscopy. Similar sensors may in

fact be used to gain further insights into these two phenomena.

In a continuous solution with an initial osmotic pressure gradient, the osmotic pressure distribution exhibits spatiotemporal evolution until an equilibrium is reached via solvent and solute diffusion. As shown in Figure 4d, this process, too, can be monitored by using the POPC-D-A liposome sensors. With a self-made device (Figure S11), an initially steep osmotic pressure gradient was generated through localized coalescence of a water drop and a drop of NaCl solution ( $\Pi \approx 0.285$  MPa, concentration of 0.375%), both containing POPC-D-A liposomes. Time-lapse emission ratio ( $R$ ) imaging enabled monitoring the evolution of the osmotic pressure distribution and of the equilibration process (Figure 4d, Figure S12a–c). At each point in space the instantaneous osmotic pressure can be calculated according to the calibration curve (Figure 3 d). This was done exemplarily inside the four rectangles indicated in Figure 4d (image on the right, recorded after 86.8 s). The obtained osmotic pressures for these four points along the osmotic gradient and over a distance of about 1 mm are 0.185, 0.138, 0.060, and 0.030 MPa, respectively, corresponding to NaCl concentrations of 0.249%, 0.189%, 0.092%, and 0.053%, respectively (Table S2). Spatially more highly resolved osmotic pressure and concentration data are reported in Figure S12d and Table S2. The steepness of the osmotic pressure gradient was found to decrease gradually with time until a constant osmotic pressure was reached after  $\approx 30$  min (Figure S12).

The spatiotemporal evolution of the FRET efficiency is in principle governed not only by the spatiotemporal evolution of the osmotic pressure, but also by the temporal response of the liposomes to osmotic pressure changes. In order to estimate the role of the latter, the temporal response of the emission ratio  $R$  was determined in “pressure-jump experiments”, where the liposomes were added to homogeneous solutions of defined osmotic pressures, followed by rapid FRET measurements. As shown in Figure S13, the equilibrium value of  $R$  is already reached when the first FRET measurement was finished after 2 s. This finding is consistent with the reported virtually “immediate” osmotic response of 1,2-dioleoyl-sn-glycero-3-phosphocholine (DOPC) liposomes<sup>[17]</sup> and suggests that the spatiotemporal evolution of the FRET efficiency indeed reflects primarily the spatiotemporal evolution of the osmotic pressure. Moreover, the time-dependent measurements also show that the emission ratio does not change within the time frame of 1 h (Figure S13), demonstrating that photobleaching does not visibly affect the data obtained under our experimental conditions.

## Conclusion

In summary, we have developed an osmotic pressure sensor based on FRET donor-acceptor loaded liposomes, which can be prepared with a simple method. It exhibits quick response and high sensitivity in measuring aqueous solutions of salt, small organic molecule, and polymer solutes. Taking advantage of fluorescence imaging, in situ spatiotemporal imaging of osmotic pressure is possible with these sensors.

This can open a path from physical chemistry to biology where osmotic gradients play an important role. This work provides a proof-of-concept for in situ measurements of osmotic pressure in dynamic systems. Further investigations on its applications in life science will be the next step.

### Acknowledgements

We thank Reinhild Dünnebacke, Carmen Remde, Andreas Fulterer from Leica company, Martina Delbianco, Giulio Fittolani and Heike Runge for their technical support in fluorescence spectroscopy, confocal microscopy, osmometry and electron microscopy. Financial support by the Max Planck Society and by the German Research Foundation via Emmy-Noether grant (SCHN 1396/1) is gratefully acknowledged. Open access funding enabled and organized by Projekt DEAL.

### Conflict of interest

The authors declare no conflict of interest.

**Keywords:** fluorescence microscopy · FRET · imaging agents · liposomes · semi-permeable membranes

- [1] W. R. G. Atkins, *Sci. Prog.* **1917**, *11*, 562–577.
- [2] S. Tokuda, A. S. L. Yu, *Int. J. Mol. Sci.* **2019**, *20*, 3513.
- [3] a) E. Han, S. S. Chen, S. M. Klisch, R. L. Sah, *Biophys. J.* **2011**, *101*, 916–924; b) S. R. Inamdar, E. Barbieri, N. J. Terrill, M. M. Knight, H. S. Gupta, *Acta Biomater.* **2019**, *97*, 437–450.
- [4] M. B. Burg, J. D. Ferraris, *J. Biol. Chem.* **2008**, *283*, 7309–7313.
- [5] M. Guo, A. F. Pegoraro, A. Mao, E. H. Zhou, P. R. Arany, Y. Han, D. T. Burnette, M. H. Jensen, K. E. Kasza, J. R. Moore, F. C. Mackintosh, J. J. Fredberg, D. J. Mooney, J. Lippincott-Schwartz, D. A. Weitz, *Proc. Natl. Acad. Sci. USA* **2017**, *114*, E8618–E8627.
- [6] a) J. Yan, C. D. Nadell, H. A. Stone, N. S. Wingreen, B. L. Bassler, *Nat. Commun.* **2017**, *8*, 327; b) A. Seminara, T. E. Angelini, J. N. Wilking, H. Vlamakis, S. Ebrahim, R. Kolter, D. A. Weitz, M. P. Brenner, *Proc. Natl. Acad. Sci. USA* **2012**, *109*, 1116–1121.
- [7] L. Beuzamy, N. Nakayama, A. Boudaoud, *Ann. Bot.* **2014**, *114*, 1517–1533.
- [8] a) A. Maroudas, *Nature* **1976**, *260*, 808–809; b) A. Maroudas, *Biophys. J.* **1968**, *8*, 575–595; c) A. Maroudas, E. Wachtel, G. Grushko, E. P. Katz, P. Weinberg, *Biochim. Biophys. Acta* **1991**, *1073*, 285–294.
- [9] A. Maroudas, C. Bannon, *Biorheology* **1981**, *18*, 619–632.
- [10] H. G. Jones, *J. Exp. Bot.* **2007**, *58*, 119–130.
- [11] D. Carrière, M. Page, M. Dubois, T. Zemb, H. Cölfen, A. Meister, L. Belloni, M. Schönhoff, H. Möhwald, *Colloids Surf. A* **2007**, *303*, 137–143.
- [12] K. Lutchmiah, A. R. D. Verliefde, K. Roest, L. C. Rietveld, E. R. Cornelissen, *Water Res.* **2014**, *58*, 179–197.
- [13] M. Macha, S. Marion, V. V. R. Nandigana, A. Radenovic, *Nat. Rev. Mater.* **2019**, *4*, 588–605.
- [14] a) M. Ballauff, *Prog. Polym. Sci.* **2007**, *32*, 1135–1151; b) C. M. Chen, S. Yang, *Polym. Int.* **2012**, *61*, 1041–1047.
- [15] J. C. Chen, Q. L. Li, M. Elimelech, *Adv. Colloid Interface Sci.* **2004**, *107*, 83–108.
- [16] a) E. R. Kay, D. A. Leigh, F. Zerbetto, *Angew. Chem. Int. Ed.* **2007**, *46*, 72–191; *Angew. Chem.* **2007**, *119*, 72–196; b) G. Saper, H. Hess, *Chem. Rev.* **2020**, *120*, 288–309.
- [17] J. Pencer, G. F. White, F. R. Hallett, *Biophys. J.* **2001**, *81*, 2716–2728.
- [18] a) H. G. Applegate, *Nature* **1960**, *186*, 232–233; b) N. P. Money, *Plant Physiol.* **1989**, *91*, 766–769.
- [19] a) H. Vink, *Eur. Polym. J.* **1974**, *10*, 149–156; b) C. Nagesh, R. P. Paily, *J. Micromech. Microeng.* **2015**, *25*, 040519.
- [20] B. L. S. Mui, P. R. Cullis, E. A. Evans, T. D. Madden, *Biophys. J.* **1993**, *64*, 443–453.
- [21] P. K. J. Kinnunen, *Cell. Physiol. Biochem.* **2000**, *10*, 243–250.
- [22] S. H. Kim, T. Y. Lee, S. S. Lee, *Small* **2014**, *10*, 1155–1162.
- [23] E. Rideau, R. Dimova, P. Schwill, F. R. Wurm, K. Landfester, *Chem. Soc. Rev.* **2018**, *47*, 8572–8610.
- [24] R. Dimova, *Adv. Colloid Interface Sci.* **2014**, *208*, 225–234.
- [25] S. Emami, W. C. Su, S. Purushothaman, V. N. Ngassam, A. N. Parikh, *Biophys. J.* **2018**, *115*, 1942–1955.
- [26] a) W. C. Su, D. L. Gettel, M. Chabanon, P. Rangamani, A. N. Parikh, *J. Am. Chem. Soc.* **2018**, *140*, 691–699; b) L. Lerebours, E. Wehrli, H. Hauser, *Biochim. Biophys. Acta Biomembr.* **1993**, *1152*, 49–60; c) S. U. A. Shibly, C. Ghatak, M. A. S. Karal, M. Moniruzzaman, M. Yamazaki, *Biophys. J.* **2016**, *111*, 2190–2201; d) E. Boroske, M. Elwenspoek, W. Helfrich, *Biophys. J.* **1981**, *34*, 95–109; e) J. Steinkuhler, R. L. Knorr, Z. Zhao, T. Bhatia, S. M. Bartelt, S. Wegner, R. Dimova, R. Lipowsky, *Nat. Commun.* **2020**, *11*, 905.
- [27] a) I. L. Medintz, T. Pons, K. Susumu, K. Boeneman, A. M. Dennis, D. Farrell, J. R. Deschamps, J. S. Melinger, G. Bao, H. Mattoussi, *J. Phys. Chem. C* **2009**, *113*, 18552–18561; b) S. Z. Wu, Y. L. Luo, F. Zeng, J. Chen, Y. N. Chen, Z. Tong, *Angew. Chem. Int. Ed.* **2007**, *46*, 7015–7018; *Angew. Chem.* **2007**, *119*, 7145–7148.
- [28] a) X. L. Zhang, Y. Xiao, X. H. Qian, *Angew. Chem. Int. Ed.* **2008**, *47*, 8025–8029; *Angew. Chem.* **2008**, *120*, 8145–8149; b) T. Pons, I. L. Medintz, K. E. Sapsford, S. Higashiyama, A. F. Grimes, D. S. English, H. Mattoussi, *Nano Lett.* **2007**, *7*, 3157–3164; c) S. Preus, L. M. Wilhelmsson, *ChemBioChem* **2012**, *13*, 1990–2001.
- [29] a) D. Srikun, E. W. Miller, D. W. Dornaille, C. J. Chang, *J. Am. Chem. Soc.* **2008**, *130*, 4596–4597; b) C. Ma, F. Zeng, L. F. Huang, S. Z. Wu, *J. Phys. Chem. B* **2011**, *115*, 874–882; c) S. R. Adams, A. T. Harootunian, Y. J. Buechler, S. S. Taylor, R. Y. Tsien, *Nature* **1991**, *349*, 694–697; d) A. Miyawaki, J. Llopis, R. Heim, J. M. McCaffery, J. A. Adams, M. Ikura, R. Y. Tsien, *Nature* **1997**, *388*, 882–887.
- [30] a) Y. Y. He, Y. Nie, G. Cheng, L. Xie, Y. Q. Shen, Z. W. Gu, *Adv. Mater.* **2014**, *26*, 1534–1540; b) S. W. A. Reulen, M. Merx, *Bioconjugate Chem.* **2010**, *21*, 860–866; c) I. L. Medintz, A. R. Clapp, H. Mattoussi, E. R. Goldman, B. Fisher, J. M. Mauro, *Nat. Mater.* **2003**, *2*, 630–638; d) J. Saha, A. D. Roy, D. Dey, S. Chakraborty, D. Bhattacharjee, P. K. Paul, S. A. Hussain, *Spectrochim. Acta Part A* **2015**, *149*, 143–149; e) T. Ng, A. Squire, G. Hansra, F. Bornancin, C. Prevostel, A. Hanby, W. Harris, D. Barnes, S. Schmidt, H. Mellor, P. I. H. Bastiaens, P. J. Parker, *Science* **1999**, *283*, 2085–2089; f) J. W. Neubauer, N. Hauck, M. J. Mannel, M. Seuss, A. Fery, J. Thiele, *ACS Appl. Mater. Interfaces* **2019**, *11*, 26307–26313.
- [31] a) J. Saha, A. D. Roy, D. Dey, J. Nath, D. Bhattacharjee, S. A. Hussain, *Sens. Actuators B* **2017**, *241*, 1014–1023; b) S. Belušáková, V. Martínez-Martínez, I. L. Arbeloa, J. Bujdák, *J. Phys. Chem. C* **2017**, *121*, 8300–8309; c) U. Gösele, M. Hauser, U. K. A. Klein, R. Frey, *Chem. Phys. Lett.* **1975**, *34*, 519–522; d) A. Muratsugu, J. Watanabe, S. Kinoshita, *J. Chem. Phys.* **2014**, *140*, 214508.
- [32] a) J. van Rheenen, M. Langeslag, K. Jalink, *Biophys. J.* **2004**, *86*, 2517–2529; b) G. W. Gordon, G. Berry, X. H. Liang, B. Levine, B. Herman, *Biophys. J.* **1998**, *74*, 2702–2713; c) A. Honda, S. R.

- Adams, C. L. Sawyer, V. Lev-Ram, R. Y. Tsien, W. R. G. Dostmann, *Proc. Natl. Acad. Sci. USA* **2001**, *98*, 2437–2442.
- [33] a) A. J. Boersma, I. S. Zuhorn, B. Poolman, *Nat. Methods* **2015**, *12*, 227–229; b) D. Gnuttt, M. Gao, O. Brylski, M. Heyden, S. Ebbinghaus, *Angew. Chem. Int. Ed.* **2015**, *54*, 2548–2551; *Angew. Chem.* **2015**, *127*, 2578–2581.
- [34] a) B. J. Litman, E. N. Lewis, I. W. Levin, *Biochemistry* **1991**, *30*, 313–319; b) S. Leekumjorn, A. K. Sum, *J. Phys. Chem. B* **2007**, *111*, 6026–6033.
- [35] A. Laouini, C. Charcosset, H. Fessi, R. G. Holdich, G. T. Vladisavljevic, *RSC Adv.* **2013**, *3*, 4985–4994.
- [36] G. T. Dempsey, J. C. Vaughan, K. H. Chen, M. Bates, X. W. Zhuang, *Nat. Methods* **2011**, *8*, 1027–1036.
- [37] Z. F. Zhang, D. Yomo, C. Gradinaru, *Biochim. Biophys. Acta Biomembr.* **2017**, *1859*, 1242–1253.
- [38] a) B. Valeur, M. N. Berberan-Santos, *Molecular Fluorescence : principles and applications*, Wiley-VCH, Weinheim, **2013**; b) J. R. Lakowicz, *Principles of Fluorescence Spectroscopy*, Springer, New York, **2013**.
- [39] a) P. H. Yancey, M. E. Clark, S. C. Hand, R. D. Bowlus, G. N. Somero, *Science* **1982**, *217*, 1214–1222; b) E. Schneck, D. Horinek, R. R. Netz, *J. Phys. Chem. B* **2013**, *117*, 8310–8321.
- [40] J. Lagerwerff, H. E. Eagle, G. Ogata, *Science* **1961**, *133*, 1486–1487.
- [41] D. L. Andrews, *Chem. Phys.* **1989**, *135*, 195–201.
- [42] P. D. Sahare, V. K. Sharma, D. Mohan, A. A. Rupasov, *Spectrochim. Acta Part A* **2008**, *69*, 1257–1264.
- [43] a) R. Lipowsky, *Nature* **1991**, *349*, 475–481; b) M. S. Long, C. D. Jones, M. R. Helfrich, L. K. Mangeney-Slavin, C. D. Keating, *Proc. Natl. Acad. Sci. USA* **2005**, *102*, 5920–5925.
- [44] C. Berney, G. Danuser, *Biophys. J.* **2003**, *84*, 3992–4010.

Manuscript received: September 2, 2020

Revised manuscript received: November 6, 2020

Accepted manuscript online: November 14, 2020

Version of record online: February 3, 2021

## Supporting Information

### **Spatiotemporal Measurement of Osmotic Pressures by FRET Imaging**

*Wenbo Zhang, Luca Bertinetti, Kerstin G. Blank, Rumiana Dimova, Changyou Gao,  
Emanuel Schneck,\* and Peter Fratzl\**

anie\_202011983\_sm\_miscellaneous\_information.pdf

## Table of Contents

1. Materials .....	1
2. Characterizations .....	1
3. Experimental methods .....	1
3.1 Emission spectra measurement of bulk dye solutions .....	1
3.2 Preparation of POPC-D-A liposomes .....	2
3.3 Osmotic strength measurement of standard solutions.....	2
3.4 Osmotic response of liposomes in solutions measured with the spectrofluorometer .....	2
3.5 Reversibility check of the osmotic response.....	2
3.6 Dynamics of the osmotic response.....	2
3.7 Confocal microscopy image acquisition and analysis .....	2
3.8 Osmotic response of liposomes in solution measured with confocal microscopy .....	2
3.9 <i>In-situ</i> osmotic pressure monitoring in the evaporation process .....	3
3.10 Spatiotemporal imaging of osmotic pressures.....	3
4. Supplementary results and schematic diagrams .....	3
4.1 Preparation diagram of POPC-D-A liposomes .....	3
4.2 DLS and PALS analysis of POPC liposomes .....	3
4.3 Förster radius of the ATTO 488 carboxy and ATTO 542 carboxy pair.....	4
4.4 Analysis of absorption and emission spectra of dye solutions .....	4
4.5 Emission ratio of dye mixture solutions .....	5
4.6 Estimate of distance between donor and acceptor dyes .....	5
4.7 Calibration curves and osmotic pressure calculation of osmotic solutions.....	6
4.8 Osmotic response of POPC-D-A sensors .....	7
4.9 Reproducibility of osmotic response of POPC-D-A sensors.....	7
4.10 Reversibility of osmotic response of POPC-D-A sensors .....	8
4.11 Spatiotemporal imaging of osmotic pressures with POPC-D-A liposomes .....	9
4.12 Dynamics of osmotic responses of POPC-D-A liposomes .....	11
References .....	11

### 1. Materials

1-palmitoyl-2-oleoyl-glycero-3-phosphocholine (POPC) was purchased from obtained from Avanti Polar Lipids (Alabaster, USA). ATTO 488 carboxy and ATTO 542 carboxy were purchased from ATTO-TEC GmbH (Siegen, Germany). Sodium chloride was purchased from neoLab Migge (Heidelberg, Germany), glycine betaine was purchased from Sigma-Aldrich (St. Luis, MO, USA), PEG20000 was purchased from Carl Roth (Karlsruhe, Germany) and chloroform was purchased from Merck KGaA (Darmstadt, Germany). The water used in all experiments was ultrapure water (18.2 M $\Omega$ ). All chemicals used in the experiments were of pharmaceutical standard and analytical grade.

### 2. Characterizations

**Size/Zeta potential** was measured with a size/ zeta potential analyzer (Zetasizer Nano-ZS, Malvern) equipped with a 532 nm He-Ne laser at room temperature (25 °C). Each value was averaged from three parallel measurements. **Ultraviolet-visible (UV-Vis) absorption spectra** were recorded with an Analytik Jena UV-Vis Specord 210 Plus spectrophotometer. **Fluorescence emission spectra** were recorded with a BioTek Cytation 5 microplate reader (bulk dye solutions) or a Horiba Fluoromax4 spectrofluorometer (dye-loaded liposomes). For UV-Vis spectra, fluorescence spectra and zeta potential/size measurements, the sample solutions were used directly. **Confocal laser scanning microscopy (CLSM)**: The liposome suspension in water was placed onto a clean glass slide, and was observed with a Leica TCS SP8 system (using commercial software). **Transmission electron microscopy (TEM)** images were recorded on a Zeiss EM 912 $\Omega$  instrument at an acceleration voltage of 120 kV. Samples were prepared by placing a drop of the liposome suspension onto a carbon film-coated copper grid and then the liposomes were stained with 1% uranyl acetate. **Cryo Scanning electron microscopy (Cryo-SEM)**: liposome suspension in water or NaCl solutions were frozen with liquid nitrogen at -210 °C from room temperature. The cryo-fixed samples were fractured at -150 °C under ultra high vacuum in a cryo-fracturing/deep etching chamber. Then the samples were sputtered with platinum, and were observed with a JEOL JSM 7500F SEM at an acceleration voltage of 3 kV.

### 3. Experimental methods

#### 3.1 Emission spectra measurement of bulk dye solutions

The emission spectra of ATTO 488 carboxy, ATTO 542 carboxy and their 1:1 mixture solutions (0.781-100  $\mu$ M) were measured with a BioTek Cytation microplate reader. The solutions were measured in a black 96-well plate with a clear glass

bottom and a clear lid (Corning CLS4580). The sample volume was 50  $\mu\text{L}$  per well. The excitation wavelength was set at 440 nm or 458 nm, and bandwidths for the excitation and emission path were both 10 nm. The microplate reader uses a front-face geometry for the fluorescence measurement, which is appropriate for relatively high concentration of dyes as used in this experiment.

### 3.2 Preparation of POPC-D-A liposomes

The POPC-D-A liposomes were prepared by the extrusion method using a Mini-Extruder (Avanti Polar Lipids Inc.). 5 mg POPC was dissolved in 0.5 mL chloroform and was evaporated by passing a gentle stream of nitrogen over the sample, followed by drying under vacuum for overnight. The lipid film was hydrated with 0.5 mL mixture solution of ATTO 488 carboxy (50  $\mu\text{M}$ ) and ATTO 542 carboxy (50  $\mu\text{M}$ ) for 1 h at 30  $^{\circ}\text{C}$ . Then the mixture was vortexed. The resulting suspension was extruded through a polycarbonate membrane (pore size 1.0  $\mu\text{m}$ ; Avanti Polar Lipids, 610010) 41 times at 30  $^{\circ}\text{C}$ . The liposomes were incubated at 4  $^{\circ}\text{C}$  overnight. Free dyes were removed by washing with centrifugal filters (Amicon Ultra-0.5 100K) (10000 g, 10 min).

### 3.3 Osmotic strength measurement of standard solutions

The NaCl, glycine betaine and PEG20000 standard solutions were prepared by weighing the solute and water at room temperature. The NaCl and glycine betaine solution osmolalities were determined from freezing point depression using an OSMOMAT 3000 Osmometer (Gonotec GmbH). Reference samples from the manufacturer (0, 300, and 850 mOsm/kg) were analyzed prior to the osmolyte samples, which were measured at least in duplicate to calibrate the osmometer. PEG20000 solution osmolalities were determined from vapor pressure depression using a VAPRO MODEL 5600 Osmometer (ELITech Group, Inc.). Reference samples from the manufacturer (100, 290 and 1000 mOsm/kg) were analyzed prior to osmolyte samples, which were measured at least in duplicate to calibrate the osmometer.

### 3.4 Osmotic response of liposomes in solutions measured with the spectrofluorometer

The POPC-D-A liposomes were dispersed in water at a concentration of 0.5 mg/mL. Then 5  $\mu\text{L}$  suspension was added to 100  $\mu\text{L}$  of the osmolyte standard solutions and the sensitized emission spectra were recorded with the spectrofluorometer (Horiba MC Fluoromax4). The excitation wavelength was set at 440 nm and the emission spectra were recorded at 450-700 nm. The bandwidths for the excitation and emission path were both 4.5 nm. The integration time was 0.1 s. The osmotic pressure of the mixture was corrected by calculating according to the osmotic pressure-mass fraction calibration curve. The (sensitized acceptor emission)/(donor emission) ratio  $R$  ( $F_{562}/F_{520}$ ) was calculated and its variation with varying osmotic pressure was analyzed to study the osmotic response of liposomes in different osmolyte solutions. The reproducibility of the osmotic response of POPC-D-A liposomes was checked by conducting two independent series of measurements with the same batch of POPC-D-A liposomes and all experimental conditions were kept the same.

### 3.5 Reversibility check of the osmotic response

5  $\mu\text{L}$  POPC-D-A liposome suspension in water (0.5 mg/mL) was added to 100  $\mu\text{L}$  of the osmolyte standard solutions and the sensitized emission spectra were recorded with the spectrofluorometer. The measurement settings were the same as above. Then water was added to dilute the solution to the desired concentration and the sensitized emission spectra of the adjusted suspension were recorded with the spectrofluorometer. The (sensitized acceptor emission)/(donor emission) ratio  $R$  ( $F_{562}/F_{520}$ ) was calculated and was analyzed to check the reversibility of the osmotic response of liposomes in different solutions.

### 3.6 Dynamics of the osmotic response

5  $\mu\text{L}$  POPC-D-A liposome suspension in water (0.5 mg/mL) was added to 100  $\mu\text{L}$  the osmolyte standard solutions. The emission (excitation wavelength 440 nm) peak intensities at 520 nm and 562 nm were recorded at indicated time with spectrofluorometer. The bandwidths for the excitation and emission path were both 4.5 nm. The integration time was 0.1 s. The (sensitized acceptor emission)/(donor emission) ratio  $R$  ( $F_{562}/F_{520}$ ) was calculated and its variation with time was analyzed.

### 3.7 Confocal microscopy image acquisition and analysis

The liposome suspensions were imaged on a Leica TCS SP8 confocal laser scanning microscope for FRET evaluation using a 10x water immersion objective. Confocal laser scanning microscopy (CLSM) allows for image acquisition of different channels pixel-per-pixel at the same time.

The FRET sensitized emission application wizard supplied by the Leica LAS AF software was used for image acquisition. The three channel settings were as follows: donor channel, excitation at 458 nm, detection at 468-538 nm; FRET channel, excitation at 458 nm, detection at 571-700 nm; acceptor channel, excitation at 561 nm, detection at 571-700 nm. All settings (HyD detector parameters (voltage, offset), pixel dwell time, laser power, electronic zoom and pinhole) were kept constant across all FRET experiments. The image sets of the samples were acquired for FRET evaluation at room temperature. In the liposomes, the donor and acceptor had a fixed 1:1 stoichiometry. Therefore, the ratio of FRET signal (sensitized acceptor emission) intensity  $F_{\text{FRET}}$  to the donor signal intensity  $F_{\text{donor}}$  was adopted as the index of FRET efficiency ( $R$ ). The pixel-by-pixel emission ratio images were obtained with the FRET sensitized emission wizard.

### 3.8 Osmotic response of liposomes in solution measured with confocal microscopy

The POPC-D-A liposomes were dispersed in water at a concentration of 2 mg/mL. Then 5  $\mu\text{L}$  suspension was added to 100  $\mu\text{L}$  standard NaCl solutions. The osmotic pressure of the mixture was corrected by calculating according to the osmotic

pressure-mass fraction calibration curve. A drop of each suspension was placed on a glass slide and was covered. The sensitized emission image sets were acquired with confocal microscopy, as stated above. For each sample, at least three image sets were recorded in different areas of the liposome suspension drop. For the calculation of the average emission ratio of the samples, the following steps were carried out. The regions of interest (ROIs) were designed as squares with a side length of 100  $\mu\text{m}$ . In the liposome suspension area of each emission ratio image, at least five evenly distributed ROIs were chosen for the calculation of apparent pixel-average emission ratio. The background values were obtained from the ROIs in the areas without liposomes in the same image. The average emission ratio was calculated by subtracting the average background value from the average apparent emission ratio. The emission ratio was plotted versus osmotic pressure to calibrate the osmotic response of liposomes in different solutions.

### 3.9 *In-situ* osmotic pressure monitoring in the evaporation process

A drop of the POPC-D-A liposome suspension (0.1 mg/mL) in 0.1351% NaCl solution (0.0946 MPa) was placed on a glass slide. In the natural evaporation process of the solution, the image sets were acquired by time-lapse imaging (time interval 1 min, duration 1 h). The emission ratios were calculated and the corresponding osmotic pressures were obtained according to the emission ratio – osmotic pressure calibration curve.

### 3.10 Spatiotemporal imaging of osmotic pressures

A drop of POPC-D-A liposome suspension (0.1 mg/mL) in 0.375% NaCl solution (0.285 MPa) and a drop of POPC-D-A liposome suspension (0.1 mg/mL) in water were placed in the two cavities of the self-made device, respectively. Then the NaCl solution was allowed to pass along the narrow passage between the two cavities and contact the water drop. To record the mixing process, the image sets were acquired by time-lapse imaging (time interval 2.14 s, duration 30 min). The emission ratios were calculated and the corresponding osmotic pressures were obtained according to the emission ratio – osmotic pressure calibration curve.

## 4. Supplementary results and schematic diagrams

### 4.1 Preparation diagram of POPC-D-A liposomes

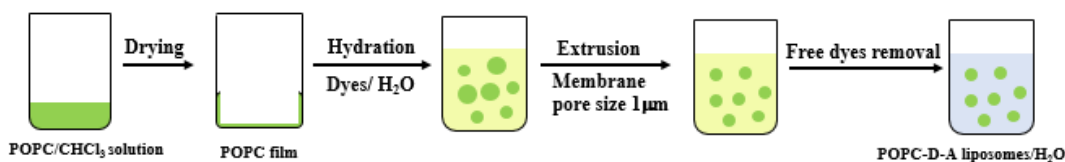


Figure S1. Schematic diagram showing the preparation method of POPC-D-A liposomes.

### 4.2 DLS and PALS analysis of POPC liposomes

The average hydrodynamic diameter of POPC liposomes in water measured by dynamic light scattering (DLS) was  $\approx 1 \mu\text{m}$  (Figure S2a) and the zeta potential measured by phase analysis light scattering (PALS) (Figure S2b) was  $\approx -21 \text{ mV}$ .

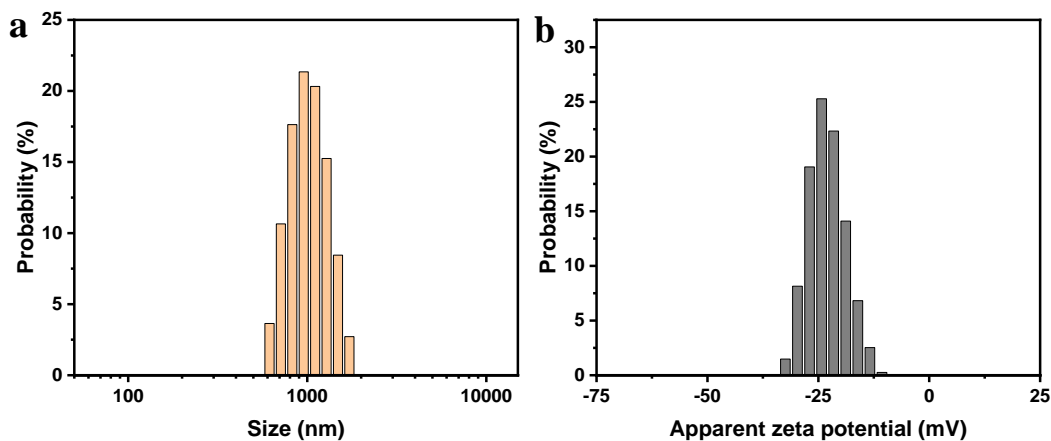


Figure S2. Distributions of size (a) and zeta potential (b) of POPC liposomes in water as obtained by dynamic light scattering (DLS) and phase analysis light scattering (PALS), respectively.

### 4.3 Förster radius of the ATTO 488 carboxy and ATTO 542 carboxy pair

Förster radius (the distance at which FRET is 50% efficient) can be calculated according to the theory developed by Förster using spectral data obtained from dilute aqueous dye solutions. The calculation equation is:

$$R_0^6 = 8.79 \times 10^{-5} (\kappa^2 n^{-4} Q_D J_{DA}(\lambda)) [\text{\AA}^6]$$

where  $\kappa^2$  represents the orientation factor,  $n$  is the solvent refractive index,  $Q_D$  is the donor molecule quantum yield (in the corresponding solvent), and  $J_{DA}(\lambda)$  is the overlap integral. The average  $\kappa^2$  ( $\kappa^2 = 2/3$  for the dye molecules with random orientation), the refractive index of water (1.33), and the ATTO 488 carboxy quantum yield (0.8) in water were used for  $R_0$  calculation. Spectral overlap was calculated according to the equation:

$$J_{DA}(\lambda) = \int_0^\infty F_{ED}(\lambda) \epsilon_{EA}(\lambda) \lambda^4 d\lambda$$

where  $F_{ED}$  is the donor (ATTO 488 carboxy) fluorescence spectrum with area normalized to unity and  $\epsilon_{EA}$  is the acceptor (ATTO 542 carboxy) molar absorption coefficient  $1.2 \times 10^5 \text{ M}^{-1} \text{ cm}^{-1}$ . The calculated  $R_0$ -value is 64 Å.

It has to be noted that in the theory given by Förster dye molecules are assumed to be so-called point-dipoles. However, in reality the diameter of a typical dye chromophore is 10 – 15 Å, which compared to typical  $R_0$ -values of 50 – 70 Å is not small.

### 4.4 Analysis of absorption and emission spectra of dye solutions

Figure 2a shows the normalized absorption and fluorescence spectra of ATTO 488 and ATTO 542 in water. The UV/Vis absorption spectra of ATTO 488 and ATTO 542 exhibited a maximum at 500 nm and 542 nm, respectively. Fluorescence emission spectra showed that maxima of ATTO 488 and ATTO 542 were centered at 520 and 562 nm, respectively, which were assigned to the dye monomers.<sup>[1]</sup>

The fluorescence spectra of ATTO 488 and ATTO 542 at a series of concentrations in water were measured with excitation wavelength fixed at 440 nm. It was observed that the fluorescence intensity of pure ATTO 488 was much higher whereas that of pure ATTO 542 is almost negligible (Figure S3). This justifies the selection of excitation wavelength (440 nm) in order to excite the donor dyes directly and to avoid the direct excitation of the acceptor dyes.

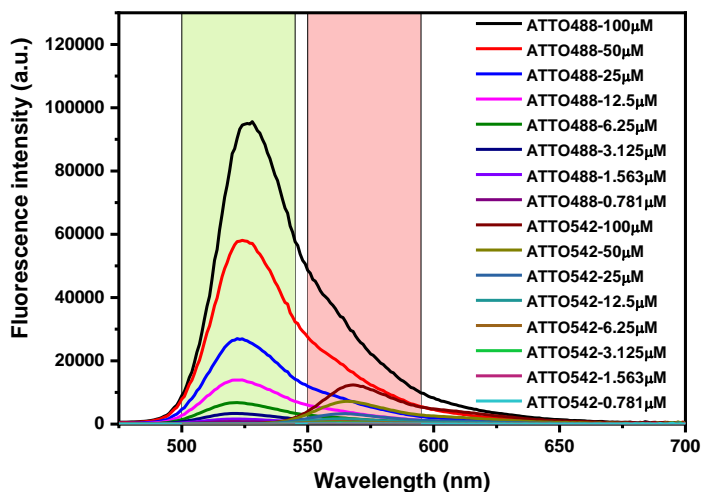


**Figure S3.** Fluorescence emission spectra of pure ATTO 488 and ATTO 542 dyes in water at different concentrations (0.781-100 μM). The excitation wavelength was 440 nm. The light green and pink shades are used to distinguish the ATTO 488 and ATTO 542 peaks, respectively.

#### 4.5 Emission ratio of dye mixture solutions

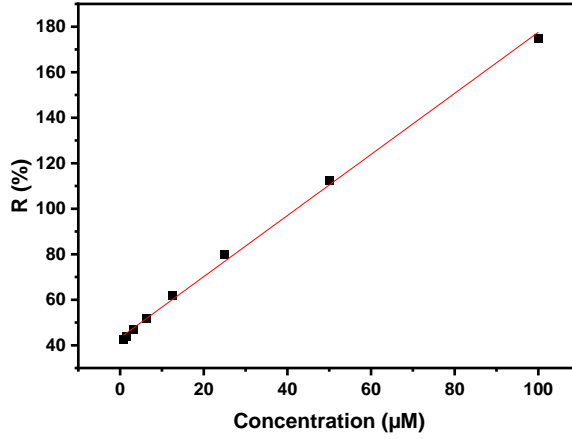


**Figure S4.** Emission ratio  $R$  as a function of the dye concentration in a 1:1 molar ratio in bulk aqueous solution. The solid line is a linear fit to the data points:  $R = 43.67 + 1.33c$  (coefficient of determination = 0.998). The excitation wavelength was 458 nm.

#### 4.6 Estimate of distance between donor and acceptor dyes

The distance between donor and acceptor dyes in a mixed solution of ATTO 488 (50  $\mu\text{M}$ ) and ATTO 542 (50  $\mu\text{M}$ ) is estimated as follows. Assume the dyes are in the ideal gas state and  $N$  particles are inside a sphere having volume  $V$ . The Wigner-Seitz radius<sup>[2]</sup> is used for the estimation.

(1) Estimate of the average distance  $r_{\text{av}}$  between two dyes in solution.

$$r_{\text{av}} = (2/3)^{1/3} a = \left(\frac{2V}{4\pi N}\right)^{1/3}, \text{ where } a = \left(\frac{3V}{4\pi N}\right)^{1/3} \text{ is the Wigner-Seitz radius.}$$

For 50  $\mu\text{M}$  this yields  $r_{\text{av}} = 17.42$  nm.

(2) Nearest neighbor distribution

The probability distribution of nearest neighbors is given by  $P(r) = \frac{3}{a} \left(\frac{r}{a}\right)^2 e^{-(r/a)^3}$ .<sup>[3]</sup>

So the probability of the dyes to be relatively close to each other ( $< 10$  nm) is

$$\int_0^{10^{-8}} P(r) dr = \int_0^{10^{-8}} \frac{3}{a} \left(\frac{r}{a}\right)^2 e^{-(r/a)^3} dr = 0.12$$

In the real mixture solution of ATTO 488 and ATTO 542, the fluorophore diffusion and the fluorophore size effect (the diameter of a typical dye chromophore is 10 – 15 Å) can result in a higher probability than the estimated. This means, the dyes have a relatively high probability ( $> 12\%$ ) to be relatively close to each other ( $< 10$  nm). And considerable FRET can occur in relatively low-concentrated donor–acceptor mixture solutions, which rationalizes the design of the osmotic pressure sensor.

#### 4.7 Calibration curves and osmotic pressure calculation of osmotic solutions

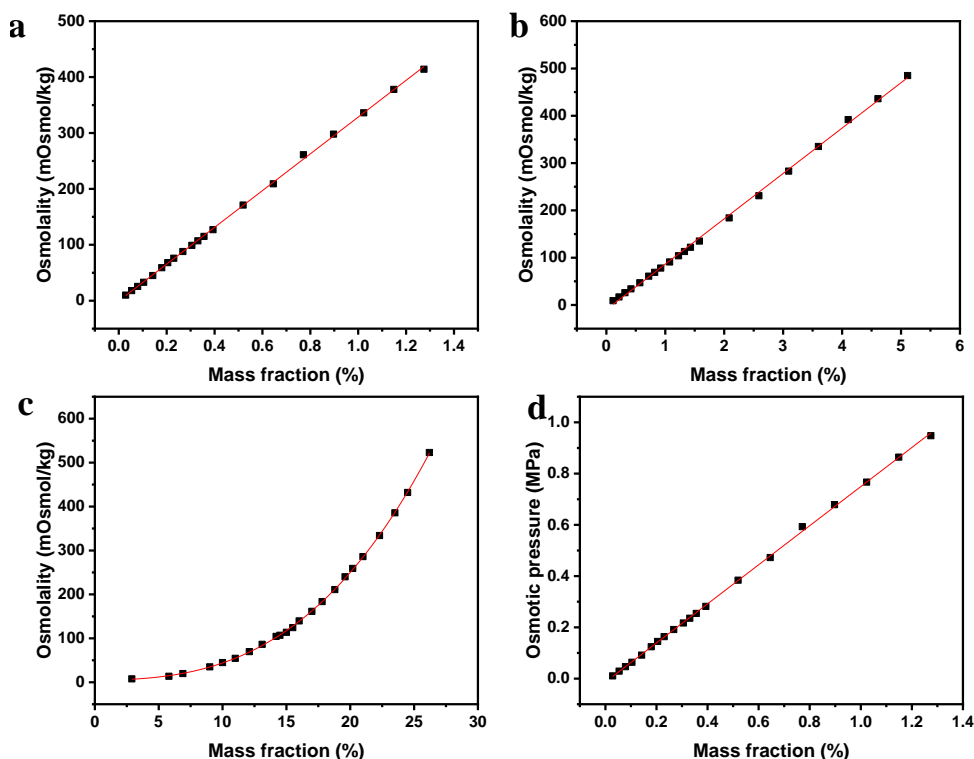


**Figure S5.** Calibration curves of osmolyte solutions. (a-c) Osmolality variation of standard NaCl (a), glycine betaine (b) and PEG 20000 (c) solutions with varying concentration measured with freezing point osmometer (a, b) and vapor pressure osmometer (c), respectively. (d) Osmotic pressure variation of standard NaCl solutions calculated based on the measured osmolalities by freezing point osmometer.

The osmolality of standard NaCl and glycine betaine solutions was measured with the freezing point osmometer. The solution osmolality versus solute mass fraction was plotted and was linearly fitted, as shown in Figure S5a,b. The fitting equation for NaCl solutions was:  $\xi = 328.83 \cdot wt\% - 0.36$ , where  $\xi$  is the osmolality (mOsmol/kg),  $wt\%$  is the mass fraction (%), coefficient of determination = 0.9996. The fitting equation for glycine betaine solutions was:  $\xi = 95.90 \cdot wt\% - 9.66$ , coefficient of determination = 0.9989. The above and the following fitting equations are applied over the range of osmolalities measured.

The osmolality of standard PEG 20000 solutions was measured with vapor pressure osmometer (34-37 °C). An equation that fits the data is the following:  $\xi = 4.28 + 0.02526 \cdot (wt\% + 1.8275)^{2.9783}$ , coefficient of determination = 0.9998 (Figure S5c).

The osmotic pressure of the standard solutions was calculated with the formula  $\Pi = \xi \cdot R \cdot T$ , where  $\Pi$  is the osmotic pressure (bar),  $\xi$  is osmolality recorded with the osmometer (Osmol/kg),  $R$  is universal gas constant 0.083145 L·bar/(mol·K),  $T$  is absolute temperature (K). Thus, at the experimental temperature of 20 °C, the osmotic pressure of the solutions can be computed from osmolality measurements and a  $\Pi$ -wt% calibration curve can be obtained (eg. Figure S5d). It has to be noted that the osmotic pressure changes non-linearly with temperature because the activities of the solutes and water change in a non-linear manner with temperature. This can result in deviations in the determination of the osmotic pressure.

#### 4.8 Osmotic response of POPC-D-A sensors

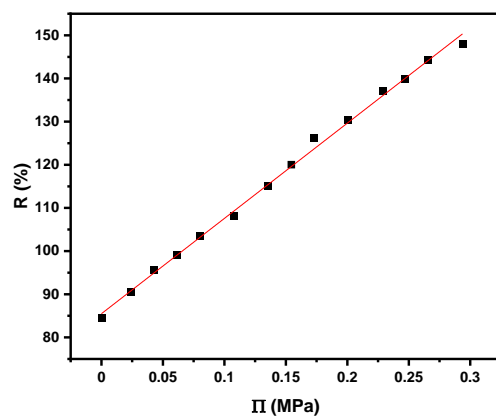


**Figure S6.** Sensing of osmotic pressures. (Sensitized acceptor emission)/(donor emission) ratio  $R$  obtained with POPC-D-A liposomes loaded with a dye concentration of  $25 \mu\text{M}$  (1:1 molar ratio) as a function of the external osmotic pressure generated by various concentrations of NaCl. Excitation wavelength: 440 nm. The solid line is an empirical linear fit to the data points (coefficient of determination = 0.997).

#### 4.9 Reproducibility of osmotic response of POPC-D-A sensors

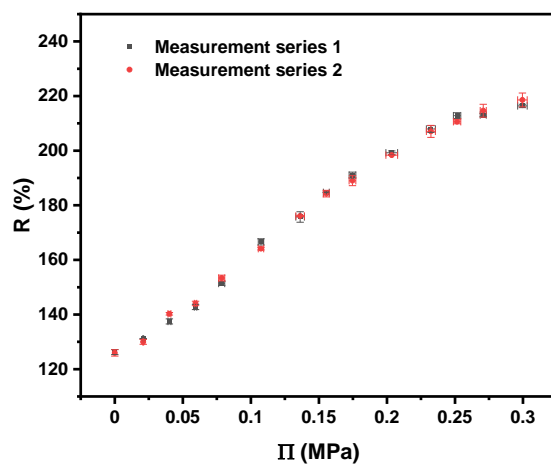


**Figure S7.** Reproducibility of osmotic response of POPC-D-A sensors. Calibration curves for osmotic pressure sensing by applying POPC-D-A liposomes (loaded with  $50 \mu\text{M}$  ATTO 488 and  $50 \mu\text{M}$  ATTO 542) in standard NaCl solutions with varying osmotic pressure  $\Pi$ . The two independent series of measurements used the same batch of POPC-D-A liposomes and all experimental conditions were the same.

#### 4.10 Reversibility of osmotic response of POPC-D-A sensors

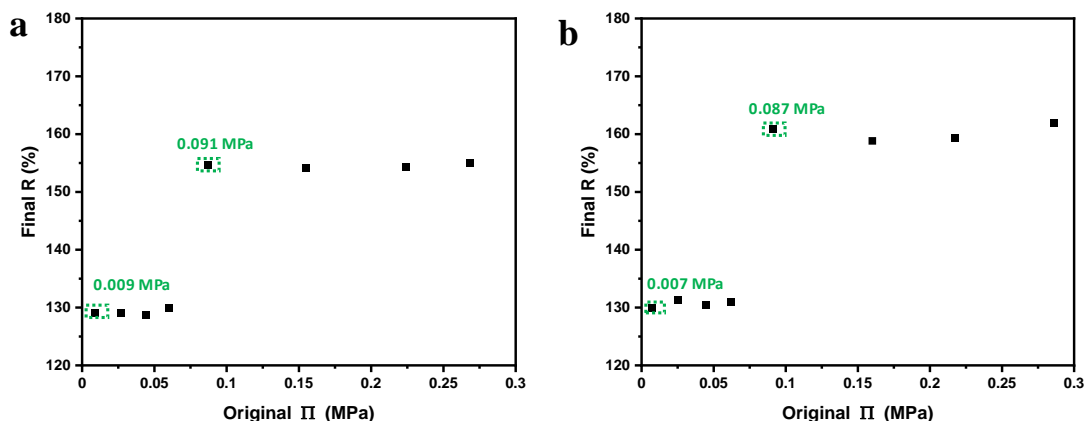


**Figure S8.** Reversibility of the osmotic response of POPC-D-A liposomes in NaCl (a) and glycine betaine (b) solutions, respectively. (a) The NaCl solutions of 0.12-0.27 MPa and 0.03-0.06 MPa containing liposomes were diluted to 0.091 MPa and 0.009 MPa, respectively. (b) The glycine betaine solutions of 0.12-0.27 MPa and 0.03-0.06 MPa containing liposomes were diluted to 0.087 MPa and 0.007 MPa, respectively. The graph's horizontal axis shows the osmotic pressures of the solutions before dilution. The vertical axis shows the emission ratio  $R$  values of the solutions after dilution.

Aqueous solutions containing POPC-D-A liposomes at various osmotic pressures in the interval  $0.12 \text{ MPa} < \Pi < 0.27 \text{ MPa}$  were re-diluted to conditions of  $\Pi = 0.091 \text{ MPa}$ , where the FRET efficiency was compared to that of POPC-D-A liposomes exposed to  $\Pi = 0.091 \text{ MPa}$  from the beginning. The same comparison was made with POPC-D-A liposomes re-diluted to conditions of  $\Pi = 0.009 \text{ MPa}$  after having been exposed to osmotic pressures in the interval  $0.03 \text{ MPa} < \Pi < 0.06 \text{ MPa}$ . As shown in Figure S8a for NaCl-based osmotic pressures and in Figure S8b for GB-based osmotic pressures, the emission ratio  $R$  values after re-dilution were consistent with those measured without having been transiently exposed to high osmotic pressures. This observation confirms that the osmotic response of POPC-D-A liposomes is reversible under the investigated experimental conditions.

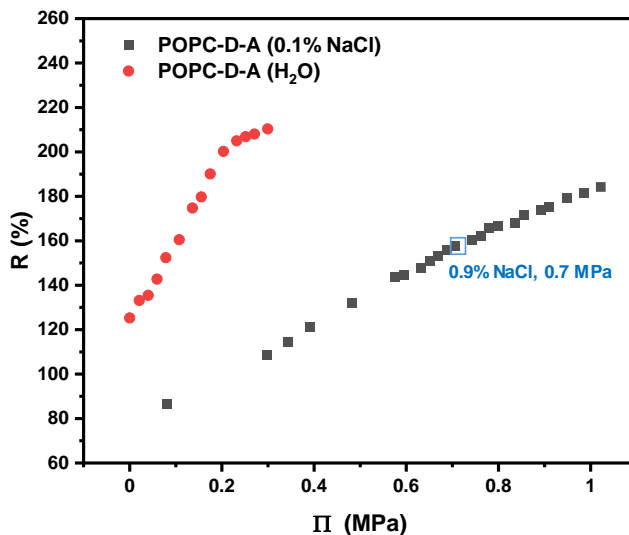


**Figure S9.** Sensing of osmotic pressures towards physiological salt range and beyond. Emission ratio  $R$  obtained with POPC-D-A (0.1% NaCl) liposomes loaded with a dye concentration of  $50 \mu\text{M}$  (1:1 molar ratio) in 0.1% (wt%) NaCl solution as a function of the external osmotic pressure generated by various concentrations of NaCl. The blue square indicates the point of 0.9% (wt%) NaCl osmotic solution of which the osmotic pressure is about 0.7 MPa. The comparison data of POPC-D-A ( $\text{H}_2\text{O}$ ) are the same as that are displayed in Figure 2d. The excitation wavelength was 440 nm.

#### 4.11 Spatiotemporal imaging of osmotic pressures with POPC-D-A liposomes

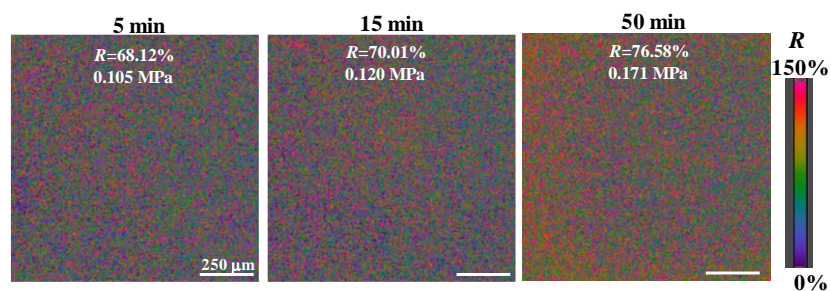


**Figure S10.** Supplementary emission ratio  $R$  images for monitoring of osmotic pressure changes of NaCl solution (0.1351%, 0.0946 MPa) during an evaporation process. The indicated osmotic pressures are calculated with the calibration curve and the measured  $R$  values

**Table S1.** Calculated osmotic pressures and NaCl concentrations in the *in-situ* monitoring of the evaporation of a NaCl solution (0.1351%, 0.0946 MPa).

Time (min)	0	5	15	45	50	55
Measured $R$ (%)	66.36	68.12	70.01	73.25	76.58	81.50
Calculated $\Pi$ (MPa)	0.091	0.105	0.120	0.145	0.171	0.228
Calculated NaCl concentration (wt%)	0.131	0.148	0.167	0.199	0.231	0.303

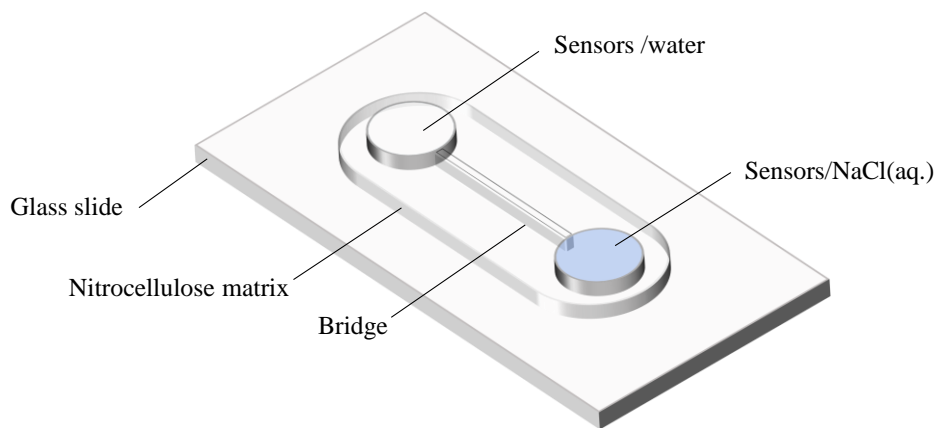


**Figure S11.** Setup for obtaining a temporal osmotic gradient. Illustration scheme of a self-made device for setting up a temporal osmotic gradient by mutual diffusion between two droplets of solutions with different osmotic pressures. The nitrocellulose matrix was set up by laying colorless and transparent nail polish on the surface of the glass slide, followed by natural drying. The two sample holders and the narrow bridge that connected the two holders were carved in the nitrocellulose matrix. A cover slip was placed on the top of the matrix to cover the holders and the passage during the experiment, so that the evaporation was neglected.

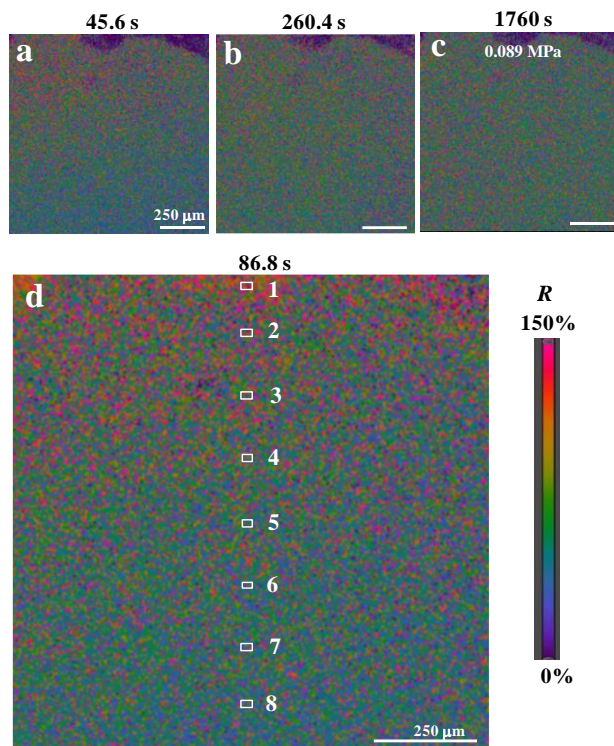


**Figure S12.** Supplementary emission ratio  $R$  images showing the osmotic pressure gradient formation by mutual diffusion of a drop of 0.375% NaCl solution (0.285MPa) and a drop of water. (a-c) The images show the *in-situ* spatiotemporal imaging of osmotic pressure gradients at indicated time points. The indicated osmotic pressure in (c) is calculated with the calibration curve and the measured  $R$  values. (d) Magnified emission ratio  $R$  image of Figure 4d-86.8 s. The osmotic pressures and concentrations at the indicated positions are shown in Table S2.

**Table S2.** Calculated osmotic pressures and NaCl concentrations in the *in-situ* spatiotemporal imaging of osmotic pressures gradients in Figure 4 d-86.8 s and Figure S12 d.

ROI No.	1	2	3	4	5	6	7	8
Measured $R$ (%)	78.34	73.69	72.29	69.47	62.41	60.97	58.48	56.66
Calculated $\Pi$ (MPa)	0.185	0.148	0.138	0.115	0.060	0.049	0.030	0.015
Calculated NaCl concentration (wt%)	0.249	0.203	0.189	0.161	0.092	0.078	0.053	0.035

#### 4.12 Dynamics of osmotic responses of POPC-D-A liposomes

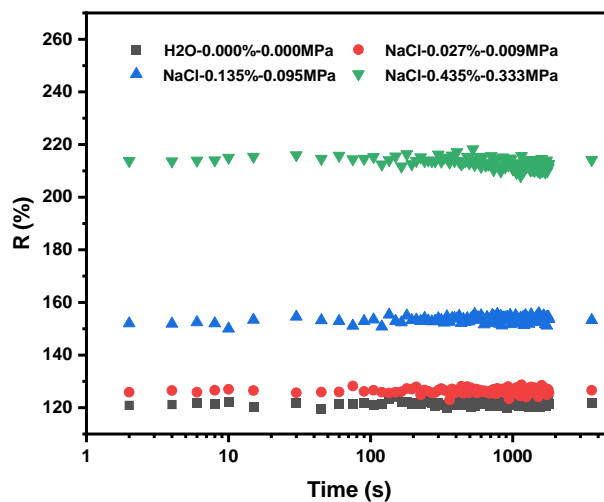


**Figure S13.** Dynamics of osmotic responses of POPC-D-A liposomes. The graph shows the monitoring of emission ratio  $R$  variation of POPC-D-A liposomes (loaded with 50  $\mu\text{M}$  ATTO 488 and 50  $\mu\text{M}$  ATTO 542) as a function of time within 1 h in water and after being applied in NaCl solutions.

#### References

- [1] a) A. Konrad, M. Metzger, A. M. Kern, M. Brecht, A. J. Meixner, *Nanoscale* **2016**, 8, 14541-14547; b) H. B. D. Thai, J. K. Yu, Y. J. Park, D. R. Ahn, *Analyst* **2015**, 140, 2804-2809; c) M. D. Wisser, S. Fischer, C. Siefe, A. P. Alivisatos, A. Salleo, J. A. Dionne, *Nano Lett.* **2018**, 18, 2689-2695.
- [2] a) L. A. Girifalco, *Statistical mechanics of solids*, Oxford University Press, Oxford; New York, **2003**; b) N. W. Ashcroft, N. D. Mermin, *Solid state physics*, Cengage Learning, New Delhi, **2019**.
- [3] a) P. Hertz, *Math. Ann. Mathematische Annalen* **1909**, 67, 387-398; b) S. Chandrasekhar, *Rev. Mod. Phys. Reviews of Modern Physics* **1943**, 15, 1-89.